Compound resonance-induced coupling effects in composite plasmonic metamaterials

Arash Farhang,[1] S. Anantha Ramakrishna,[2] and Olivier J. F. Martin[1,*]

[1]*Nanophotonics and Metrology Laboratory, Swiss Federal Institute of Technology Lausanne EPFL-STI-NAM, Station 11, CH-1015 Lausanne, Switzerland*

[2]*Metamaterials and Plasmonics Laboratory, Department of Physics, Indian Institute of Technology Kanpur, 208016 Kanpur, India*

[*]*olivier.martin@epfl.ch*

Abstract: We study a compound plasmonic system composed of a periodic Au grating array placed close to a thin Au film. The study is not limited to normal incidence and dispersion diagrams are computed for a broad variety of parameters. In addition to identifying localized and propagating modes and the coupling/hybridization interactions between them, we go further and identify modes of compound nature, i.e. those exhibiting both localized and propagating characteristics, and discuss which plasmon modes can exhibit such a behavior in the system at hand and how structural parameters play a central part in the spectral response of such modes.

OCIS codes: (250.5403) Plasmonics; (240.6680) Surface plasmons; (160.3918) Metamaterials.

References and links

1. P. Berini, "Plasmon polariton modes guided by a metal film of finite width," Opt. Lett. **24**(15), 1011–1013 (1999).
2. P. Berini, R. Charbonneau, and N. Lahoud, "Long-range surface plasmons on ultrathin membranes," Nano Lett. **7**(5), 1376–1380 (2007).
3. G. Colas des Francs, J. Grandidier, S. Massenot, A. Bouhelier, J.-C. Weeber, and A. Dereux, "Integrated plasmonic waveguides: A mode solver based on density of states formulation," Phys. Rev. B **80**(11), 115419 (2009).
4. A. Degiron, S.-Y. Cho, C. Harrison, N. M. Jokerst, C. Dellagiacoma, O. J. F. Martin, and D. R. Smith, "Experimental comparison between conventional and hybrid long-range surface plasmon waveguide bends," Phys. Rev. A **77**(2), 021804 (2008).
5. A. Degiron, S.-Y. Cho, T. Tyler, N. M. Jokerst, and D. R. Smith, "Directional coupling between dielectric and long-range plasmon waveguides," New J. Phys. **11**(1), 015002 (2009).
6. D. K. Gramotnev and S. I. Bozhevolnyi, "Plasmonics beyond the diffraction limit," Nat. Photonics **4**(2), 83–91 (2010).
7. J. Homola, S. S. Yee, and G. Gauglitz, "Surface plasmon resonance sensors: review," Sens. Actuators B Chem. **54**(1-2), 3–15 (1999).
8. J. Chen, D. Wang, J. Xi, L. Au, A. Siekkinen, A. Warsen, Z.-Y. Li, H. Zhang, Y. Xia, and X. Li, "Immuno gold nanocages with tailored optical properties for targeted photothermal destruction of cancer cells," Nano Lett. **7**(5), 1318–1322 (2007).
9. A. M. Gobin, M. H. Lee, N. J. Halas, W. D. James, R. A. Drezek, and J. L. West, "Near-infrared resonant nanoshells for combined optical imaging and photothermal cancer therapy," Nano Lett. **7**(7), 1929–1934 (2007).
10. L. R. Hirsch, R. J. Stafford, J. A. Bankson, S. R. Sershen, B. Rivera, R. E. Price, J. D. Hazle, N. J. Halas, and J. L. West, "Nanoshell-mediated near-infrared thermal therapy of tumors under magnetic resonance guidance," Proc. Natl. Acad. Sci. U.S.A. **100**(23), 13549–13554 (2003).
11. D. P. O'Neal, L. R. Hirsch, N. J. Halas, J. D. Payne, and J. L. West, "Photo-thermal tumor ablation in mice using near infrared-absorbing nanoparticles," Cancer Lett. **209**(2), 171–176 (2004).
12. J. N. Anker, W. P. Hall, O. Lyandres, N. C. Shah, J. Zhao, and R. P. Van Duyne, "Biosensing with plasmonic nanosensors," Nat. Mater. **7**(6), 442–453 (2008).
13. T. Rindzevicius, Y. Alaverdyan, A. Dahlin, F. Höök, D. S. Sutherland, and M. Käll, "Plasmonic sensing characteristics of single nanometric holes," Nano Lett. **5**(11), 2335–2339 (2005).
14. L. J. Sherry, R. Jin, C. A. Mirkin, G. C. Schatz, and R. P. Van Duyne, "Localized surface plasmon resonance spectroscopy of single silver triangular nanoprisms," Nano Lett. **6**(9), 2060–2065 (2006).
15. A. Unger, U. Rietzler, R. Berger, and M. Kreiter, "Sensitivity of crescent-shaped metal nanoparticles to attachment of dielectric colloids," Nano Lett. **9**(6), 2311–2315 (2009).
16. W. Zhang, L. Huang, C. Santschi, and O. J. F. Martin, "Trapping and sensing 10 nm metal nanoparticles using plasmonic dipole antennas," Nano Lett. **10**(3), 1006–1011 (2010).

#175682 - $15.00 USD Received 6 Sep 2012; revised 19 Nov 2012; accepted 29 Nov 2012; published 19 Dec 2012

17. G. Lévêque and O. J. F. Martin, "Narrow-band multiresonant plasmon nanostructure for the coherent control of light: an optical analog of the xylophone," Phys. Rev. Lett. **100**(11), 117402 (2008).
18. D. Brunazzo, E. Descrovi, and O. J. F. Martin, "Narrowband optical interactions in a plasmonic nanoparticle chain coupled to a metallic film," Opt. Lett. **34**(9), 1405–1407 (2009).
19. J. Cesario, M. U. Gonzalez, S. Cheylan, W. L. Barnes, S. Enoch, and R. Quidant, "Coupling localized and extended plasmons to improve the light extraction through metal films," Opt. Express **15**(17), 10533–10539 (2007).
20. J. Cesario, R. Quidant, G. Badenes, and S. Enoch, "Electromagnetic coupling between a metal nanoparticle grating and a metallic surface," Opt. Lett. **30**(24), 3404–3406 (2005).
21. A. Christ, G. Lévêque, O. J. F. Martin, T. Zentgraf, J. Kuhl, C. Bauer, H. Giessen, and S. G. Tikhodeev, "Near-field-induced tunability of surface plasmon polaritons in composite metallic nanostructures," J. Microsc. **229**(2), 344–353 (2008).
22. Y. Chu and K. B. Crozier, "Experimental study of the interaction between localized and propagating surface plasmons," Opt. Lett. **34**(3), 244–246 (2009).
23. J. DiMaria and R. Paiella, "Plasmonic dispersion engineering of coupled metal nanoparticle-film systems," J. Appl. Phys. **111**(10), 103102 (2012).
24. F. Le, N. Z. Lwin, N. J. Halas, and P. Nordlander, "Plasmonic interactions between a metallic nanoshell and a thin metallic film," Phys. Rev. B **76**(16), 165410 (2007).
25. G. Lévêque and O. J. F. Martin, "Optical interactions in a plasmonic particle coupled to a metallic film," Opt. Express **14**(21), 9971–9981 (2006).
26. G. Lévêque and O. J. F. Martin, "Tunable composite nanoparticle for plasmonics," Opt. Lett. **31**(18), 2750–2752 (2006).
27. N. Liu, H. Guo, L. Fu, S. Kaiser, H. Schweizer, and H. Giessen, "Plasmon hybridization in stacked cut-wire metamaterials," Adv. Mater. (Deerfield Beach Fla.) **19**(21), 3628–3632 (2007).
28. J. J. Mock, R. T. Hill, A. Degiron, S. Zauscher, A. Chilkoti, and D. R. Smith, "Distance-dependent plasmon resonant coupling between a gold nanoparticle and gold film," Nano Lett. **8**(8), 2245–2252 (2008).
29. J. J. Mock, R. T. Hill, Y.-J. Tsai, A. Chilkoti, and D. R. Smith, "Probing dynamically tunable localized surface plasmon resonances of film-coupled nanoparticles by evanescent wave excitation," Nano Lett. **12**(4), 1757–1764 (2012).
30. P. Nordlander and E. Prodan, "Plasmon hybridization in nanoparticles near metallic surfaces," Nano Lett. **4**(11), 2209–2213 (2004).
31. N. Papanikolaou, "Optical properties of metallic nanoparticle arrays on a thin metallic film," Phys. Rev. B **75**(23), 235426 (2007).
32. K. Wang, E. Schonbrun, and K. B. Crozier, "Propulsion of gold nanoparticles with surface plasmon polaritons: Evidence of enhanced optical force from near-field coupling between gold particle and gold film," Nano Lett. **9**(7), 2623–2629 (2009).
33. J. Ye, M. Shioi, K. Lodewijks, L. Lagae, T. Kawamura, and P. Van Dorpe, "Tuning plasmonic interaction between gold nanorings and a gold film for surface enhanced Raman scattering," Appl. Phys. Lett. **97**(16), 163106 (2010).
34. J. Aizpurua, P. Hanarp, D. S. Sutherland, M. Käll, G. W. Bryant, and F. J. García de Abajo, "Optical properties of gold nanorings," Phys. Rev. Lett. **90**(5), 057401 (2003).
35. J. J. Mock, M. Barbic, D. R. Smith, D. A. Schultz, and S. Schultz, "Shape effects in plasmon resonance of individual colloidal silver nanoparticles," J. Chem. Phys. **116**(15), 6755–6759 (2002).
36. G. Lévêque and O. J. F. Martin, "Optimization of finite diffraction gratings for the excitation of surface plasmons," J. Appl. Phys. **100**, 124301 (2006).
37. H. Raether, "Surface plasmons on smooth and rough surfaces and on gratings," Springer Tracts Mod. Phys. **111**, 1–133 (1988).
38. P. B. Johnson and R. W. Christy, "Optical constants of the nobel metals," Phys. Rev. B **6**(12), 4370–4379 (1972).
39. B. Gallinet, A. M. Kern, and O. J. F. Martin, "Accurate and versatile modeling of electromagnetic scattering on periodic nanostructures with a surface integral approach," J. Opt. Soc. Am. A **27**(10), 2261–2271 (2010).
40. A. M. Kern and O. J. F. Martin, "Surface integral formulation for 3D simulations of plasmonic and high permittivity nanostructures," J. Opt. Soc. Am. A **26**(4), 732–740 (2009).
41. A. M. Kern and J. F. Olivier, "Modeling near-field properties of plasmonic nanoparticles: a surface integral approach," in *SPIE Optics + Photonics 2009*, 2009), 739518–739511.
42. P. Berini, "Long-range surface plasmon polaritons," Adv. Opt. Photon. **1**(3), 484–588 (2009).
43. S. A. Maier, *Plasmonics: Fundamentals and Applications* (Spinger-Verlag, 2007).
44. J. P. Kottmann, O. J. F. Martin, D. R. Smith, and S. Shultz, "Field polarization and polarization charge distributions in plasmon resonant nanoparticles," New J. Phys. **2000**, 2 (2000).
45. B. E. A. Saleh and M. C. Teich, "Guided-Wave Optics," in *Fundamentals of Photonics* (John Wiley & Sons, Inc., 2001), pp. 238–271.
46. A. Farhang and O. J. F. Martin, "Plasmon delocalization onset in finite sized nanostructures," Opt. Express **19**(12), 11387–11396 (2011).

#175682 - $15.00 USD Received 6 Sep 2012; revised 19 Nov 2012; accepted 29 Nov 2012; published 19 Dec 2012

1. Introduction

Plasmonics, the bridge between the best of optics and electronics, is based on resonant electron plasma oscillations in metallic nanostructures. In the most basic sense, two types of plasmon resonances exist, delocalized plasmons and localized plasmons. The former, based on the free propagation of surface waves at an extended metal dielectric interface (e.g. a conductive film), shows great promise in the development of ultra-fast and compact optical circuitry [1–6] and has played a major role in the development of surface plasmon based biosensors [7]. The latter, confined around nanoparticles, nanoantennas, and various other compact nanostructures, allows for very high near-field enhancements at optical frequencies due to high localizations of the scattered field and has been shown useful in applications ranging from cancer treatment [8–11] to trapping and sensing [12–16]. In the last few years, great attention has been devoted to studying systems composed of not only localized metallic nanostructures or a conductive film, but rather composed of both [17]. The interaction and hybridization of localized surface plasmon resonances (LSPRs) and propagating surface plasmon resonances (SPPs) in such systems results in a variety of rich and interesting optical phenomena [17–33].

For a given metal, environmental condition, planewave illumination, and compact system where retardation does not play a significant role, the resonant response of localized plasmon modes depends primarily on the structural geometry [34, 35]. The resonant response of a conductive film, however, depends not only on the structural geometry, i.e. the film thickness, but also on the orientation of the excitation source, specifically the incident k-vector matching conditions [36, 37]. Thus for a system composed of a metallic nanostructure in close proximity to a conductive film, one naturally expects that under the right coupling conditions, the resonant response of a given mode depends not only on the structural parameters of the nanostructure or on the excitation conditions, but rather upon both factors. Most studies, however, have focused primarily on normally incident excitation. Here we investigate excitation at a wide range of incidence angles and wavelengths. We observe not only the coupling/hybridization between localized and propagating modes, but also investigate whether such modes themselves have a compound nature, i.e. exhibit both properties of localized and propagating plasmon modes due to near-field coupling effects.

The paper is organized in the following manner: after quickly introducing the geometry of the plasmonic structure and the computational method used in Section 2, the three basic resonances of the system are identified in Section 3. The compound nature and coupling/hybridization of these resonances is then discussed in Section 4, and finally a conclusion is made in Section 5 with a summary of the results.

2. Geometry and method

The geometry under study consists of a single Au grating layer of period Λ = 200nm placed a distance s = 20nm from the surface of a continuous Au film of thickness t = 25nm. We use the dielectric constant of Au obtained by Johnson and Christy [38]. The entire structure is embedded within a silica (SiO_2) matrix with a dielectric permittivity of ε = 2.13. The length of each grating element/particle in the array is varied between l = 50-150nm, the widths are set to w = 15nm, and the entire structure is invariant along the y-axis. The system is excited via p-polarized planewave illumination (H-field oriented along the grating lines), as shown schematically in Fig. 1, over a range of wavelengths λ = 400-1200nm and angles θ = 0-85° with respect to the normal.

The simulation method used in this paper is based on the Surface Integral Equation (SIE) technique, extended for use in periodic structures. This method is particularly useful as it decreases the computation time significantly through surface rather than volume meshing and also allows for calculation of the electromagnetic field arbitrarily close to or far from the structure being studied, as well as within the structure [39–41]. With this we obtain the absorption of radiation in the structure via calculated far-field reflection and transmission spectra. The near field of the structure is then investigated at the corresponding angles and

#175682 - $15.00 USD Received 6 Sep 2012; revised 19 Nov 2012; accepted 29 Nov 2012; published 19 Dec 2012

wavelengths of the multiple resonant absorption peaks in order to determine the nature of each resonance.

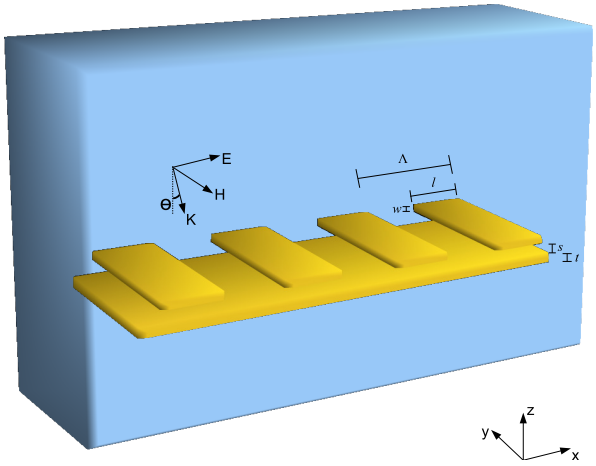

Fig. 1. The geometry being studied, a plasmonic system composed of a periodic Au grating layer above a Au film. The structural parameters used in this study are s = 20nm, t = 25nm, l = 50-150nm, w = 15nm, a background of glass with a permittivity of ε = 2.13, and a periodicity of Λ = 200nm.

3. Identification of the plasmonic modes

For the system being studied we expect two families of modes, the first being the localized plasmon modes supported by the particles and the second being the propagating SPP modes of the continuous Au film. In this case, where we have a film of small thickness (t = 25nm) embedded in silica, the SPP modes on the two sides of the film couple, resulting in two distinct SPP modes, one where the charge distribution on the two sides of the film is symmetric (even mode, or short-range mode) and another where it is antisymmetric (odd mode, or long-range mode) [42, 43].

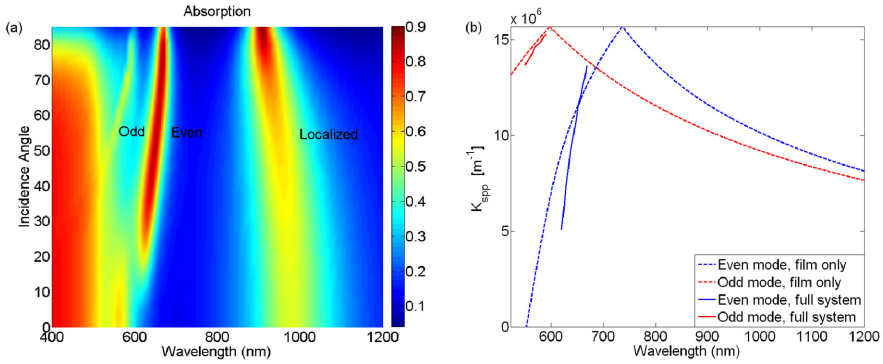

Fig. 2. Absorption spectra and SPP dispersions of the system shown in Fig. 1. (a) Absorption spectra for a particle length of l = 100nm, showing three absorption bands at λ = 550nm, 660nm, and 970nm for θ = 55° incidence that correspond to the odd and even SPP modes of the film and the localized dipole-image mode of the particles, respectively. (b) Calculated dispersion curves for even and odd SPP modes on a plain Au film folded back into the first Brillouin zone (Λ = 200nm periodicity) and matched dispersion curves extracted from panel (a) for even and odd SPP modes of the full grating and film system assuming m = –1 Bragg scattering.

#175682 - $15.00 USD Received 6 Sep 2012; revised 19 Nov 2012; accepted 29 Nov 2012; published 19 Dec 2012

We plot in Fig. 2(a) the calculated absorption spectra for a Au grating layer s = 20nm above the continuous Au film. The spectra show three distinct absorption bands for wavelengths λ > 500nm. Below λ = 500nm the system is plagued by the intrinsic losses of Au. The band at a larger wavelength of λ = 970nm for θ = 55° incidence is the localized dipole mode of the grating elements coupled to their mirror image in the Au film [25]. To verify this fact we display in Figs. 3(a), 3(b) the total electric field amplitude in an x-z cross section of the grating-film structure, and the polarization charge distribution, respectively (the polarization charges are proportional to the divergence of the electric field at the Au-SiO_2 interface) [44]. Vector arrows in all figures show the electric field orientation. Note all such figures in this paper show the electric field profile and charge distributions at the instant when the maximum field amplitude occurs. Movies linked via these figures show the periodic time evolution of these modes. In Figs. 3(a), 3(b) these animations verify the nature of this resonance as a dipolar mode of the grating elements coupled to their mirror image within the Au film. We will refer to this mode here on as simply localized dipole-image mode. In contrast, the two bands at lower wavelengths of λ = 550nm and 660nm for θ = 55° incidence are those corresponding to the even and odd SPP modes respectively.

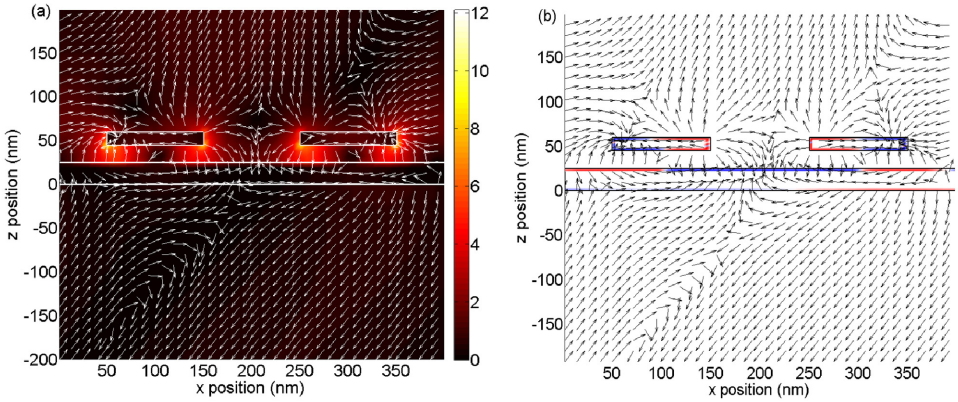

Fig. 3. Cross section of the system shown in Fig. 1, with l = 100nm, showing a snapshot of (a) the electric field amplitude (Media 1) and (b) the normalized polarization charge distribution when the field is at a maximum (Media 2). The arrows indicate the orientation of the electric field, while the color scale indicates the amplitude of the field and the distribution of positive (red) and negative (blue) charges. Clearly this is the dipole mode of the particle coupled to its mirror image in the Au film. The media files illustrate how the field and charges vary in time and thus the nature of the resonance. Planewave excitation at θ = 55° incidence and λ = 970nm.

At first glance one would expect the two SPP modes to disperse in the opposite direction than that shown in Fig. 2(a), decreasing wavelength with increasing angle of incidence. These modes, however, are the m = –1 Bragg scattered SPP modes and thus disperse in the opposite direction. To verify this claim, the following is plotted in Fig. 2(b): first, the dispersion of the SPP modes are calculated analytically [45] for a simple 25nm thick Au film in SiO_2 and folded back into the first Brillouin zone assuming a Λ = 200nm periodicity. Second, all values for k_{spp} possible via grating excitation are calculated from Eq. (1) [37], assuming m = ± 1:

$$k_{spp} = \sqrt{\varepsilon_{SiO_2}}\frac{2\pi}{\lambda}\sin\theta + m\frac{2\pi}{\Lambda} \qquad (1)$$

For m = 1, k_{spp} > 3x10^7 m^{-1} are obtained, much too large to match the analytically calculated SPP curves, which indicate k_{spp} < 3x10^7 m^{-1}. For m = –1, however, values of k_{spp} < 3x10^7 m^{-1} are obtained. Thus, the angular and spectral position of the absorption peaks of the two SPP modes are subsequently matched up with the corresponding k_{spp} values for m = –1, translated into the first Brilliouin zone, and plotted in Fig. 2(b). As can be seen, these match

#175682 - $15.00 USD Received 6 Sep 2012; revised 19 Nov 2012; accepted 29 Nov 2012; published 19 Dec 2012

well with the analytically calculated curves of a plain Au film, particularly for the case of the odd SPP mode. Further simulations with dielectric gratings having a large permittivity contrast with respect to the silica matrix have shown excitation of the same two SPP modes, thereby verifying that the modes can be excited via Bragg scattering. Additional simulations with large permittivity contrast also show much better excitation of the odd SPP mode than is seen here, as one would naturally expect.

Physically, the folding back of the two modes into the first Brillouin zone means that the incident light is scattered backwards rather than forwards, resulting in a reverse propagating SPP wave. This can be seen in the movie files linked by Figs. 4(a)-4(d), where we display the time varying electric field amplitude and polarization charges in an x-z cross section of the grating-film structure like in Figs. 3(a), 3(b). Notice that the field vectors within the Au film exhibit a symmetric distribution for the even mode and an antisymmetric distribution for the odd mode as is expected. Furthermore, the SPP propagation direction is reversed with respect to the incident field.

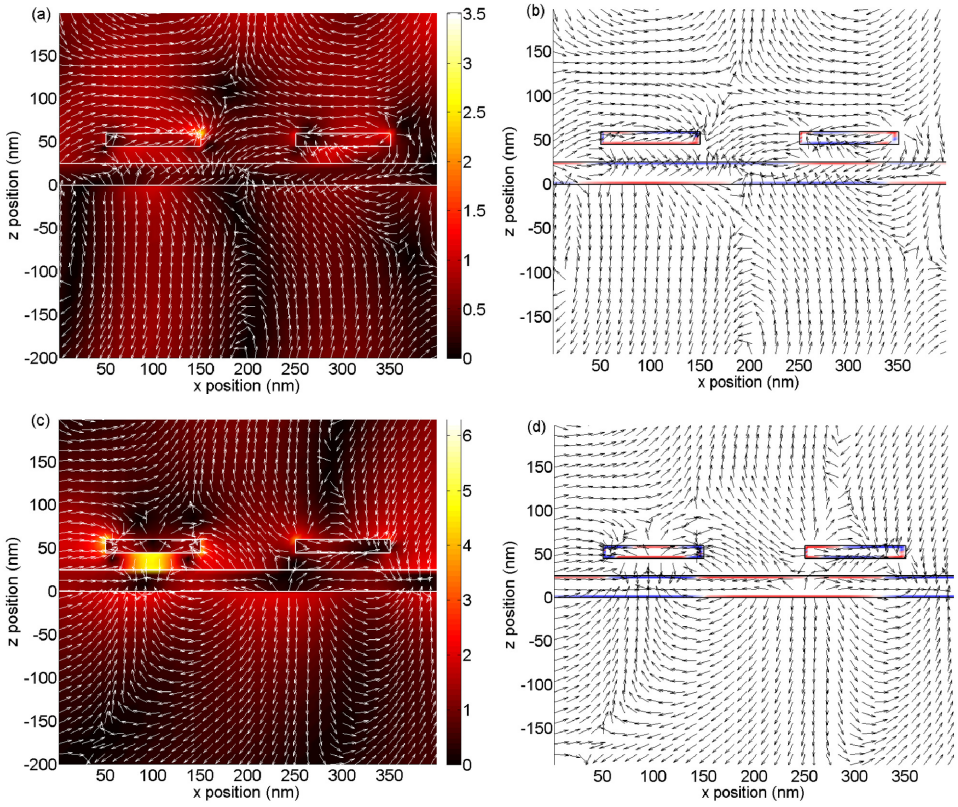

Fig. 4. Cross sections of the system shown in Fig. 1 with l = 100nm, showing (a) (Media 3), (c) (Media 5) time varying electric field amplitude and (b) (Media 4), (d) (Media 6) polarization charges. (a), (b) Odd SPP mode for a θ = 55° incidence planewave excitation, λ = 550nm. (c), (d) Even SPP mode for a θ = 55° incidence planewave excitation, λ = 660nm. The linked media files show the time evolution of the field amplitude and polarization charges.

4. Compound nature of plasmonic modes

An interesting feature that can be seen in Figs. 4(c), 4(d) is that the field profile for the even SPP mode, which resembles horizontally oriented dipoles of switching orientation within the Au film [46], induces anti-parallel oriented dipoles within each grating element, thereby resulting in effectively a quadrupole mode coupled to its mirror image, i.e. an octupole mode

#175682 - $15.00 USD Received 6 Sep 2012; revised 19 Nov 2012; accepted 29 Nov 2012; published 19 Dec 2012

as the SPP wave propagates along the Au film. Note, that quadrapole resonance seen here is a pair of opposing dipoles oriented and positioned along the length of the particle and should not be confused with the often seen case of two opposing dipoles, with one along the top edge of the particle and the other along the bottom edge. Additional simulations of absorption spectra shown in Fig. 5 for increasing particle lengths of l = 100-150nm, while keeping the period constant at Λ = 200nm, and a incidence of θ = 55⌋ reveal a red-shifting of this mode with incremental increases in the particle length, just like that of the localized dipole-image mode of the grating elements. This shows that the mode is not only a Bragg scattered SPP mode, but rather an SPP mode of compound nature, i.e. exhibiting properties of both localized and propagating plasmon modes (we refer to this specific mode from here on as the even-compound SPP mode). This can also explain the mismatches seen in the dispersion of this mode and that of a plain Au film, particularly why the dispersion of the even-compound SPP mode for this Au grating and film system is flatter (a usual characteristic of localized modes) than that of just a plain Au film.

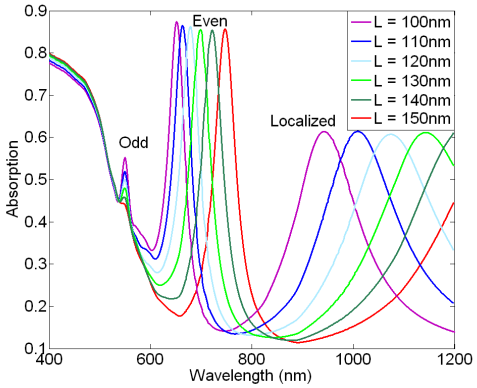

Fig. 5. Absorption spectra of the system shown in Fig. 1, as a function of particle length from l = 100-150nm, while keeping the period constant to Λ = 200nm, for θ = 55° incidence. Note the redshifting of the localized dipole-image mode and also that of the even-compound SPP mode with increasing particle length.

Furthermore, field profile and charge distribution plots shown in Figs. 6(a), 6(b) respectively for the same even-compound SPP resonance now positioned at λ = 680nm given a length l = 120nm and an incidence θ = 55°, display a much clearer view of the quadrapole that is supported along the length of the particle. This is simply because shorter particles cannot as easily support this quadrapolar charge distribution as longer particles. In fact, as will be shown in Figs. 7(c), 7(d), at a much shorter length of l = 50nm, the field profile and charge distribution of the same peak display instead a dipolar orientation along the length of the particle. In contrast to this size dependent modal and spectral response, the odd SPP mode is almost purely dependant on Bragg scattering and thus its resonance position stays almost constant with the same increase in particle length (Fig. 5). The absorption peak, however, decreases in strength with increasing particle length. This is simply due to the fact that an increase in particle length leads to a loss in symmetry on the two sides of the Au film.

#175682 - $15.00 USD Received 6 Sep 2012; revised 19 Nov 2012; accepted 29 Nov 2012; published 19 Dec 2012

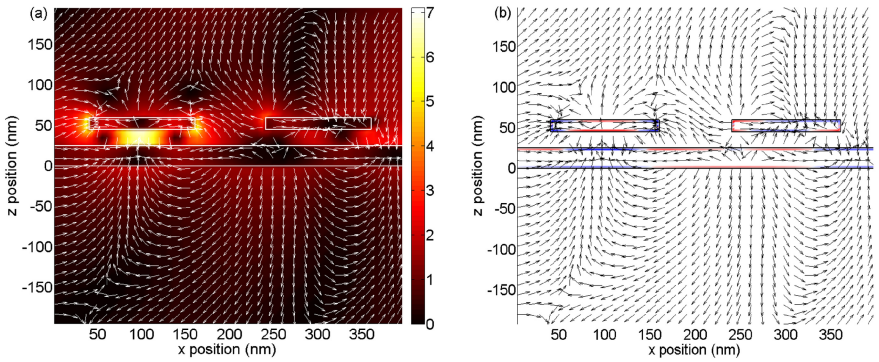

Fig. 6. Cross section of the system shown in Fig. 1 with l = 120nm, showing (a) the time varying electric field amplitude (Media 7) and (b) polarization charges (Media 8) for a θ = 55° incidence planewave excitation and λ = 680nm, corresponding to the even-compound SPP mode. Note, in contrast to the field and charge profiles for l = 100nm (Figs. 4(c)-4(d)), here for l = 120nm, the quadrapolar nature of this mode is much more distinctly visible, due to the elongation in the particle length.

The effective nature of the even-compound SPP mode as a propagating surface wave and simultaneously a quadrapole mode coupled to its mirror image has a limit as the particle length is decreased below l = 100nm. One intuitively can see that below a certain size, the grating elements will be too small to support a quadrupole as the SPP propagates by. At this stage the polarization charges within the grating elements will be primarily dipolar rather than quadrapolar. To illustrate this fact, we show in Figs. 7(a)-7(d) calculated field profile and polarization charge plots at the resonance peaks corresponding to the even-compound SPP mode and localized dipole-image mode referred to in Fig. 2(a) and Fig. 5, but for a grating size of l = 50nm. As can be seen, the two peaks at λ = 610nm and 700nm, respectively, for θ = 55⌋ incidence, exhibit the characteristics of a compound plasmonic mode, with both displaying a localized dipole-image resonance as well as a simultaneous backward propagating SPP mode. Referring to the calculated absorption spectra for l = 50nm, Fig. 8(a), we see that the large spectral shift of the localized dipole-image mode towards the blue has brought it in close proximity to the even SPP mode, thus resulting in a coupling/hybridization of the two. As can be seen in Figs. 7(b), 7(d), this hybridization results in a parallel combination of the localized dipole-image mode and the even SPP mode at a higher energy/lower wavelength of λ = 610nm and an anti-parallel combination at a lower energy/higher wavelength of λ = 700nm respectively. In the anti-parallel combination (Fig. 7(d)), the dipole in the particle is anti-parallel to the charges of the even SPP mode in the Au film and thus the induced image charges of the dipole follow/are parallel to those of the even SPP mode, hence a fully symmetric charge distribution is seen in the Au film. In the parallel combination, however, the induced/forced image charges are opposite/anti-parallel to those of the even SPP mode thereby resulting in the observed asymmetry in the charge distribution between the two surfaces of the Au film (Fig. 7(b)). It is interesting to note, however, that despite this hybridization, the field profile at the higher resonance wavelength of λ = 700nm (Fig. 7(c)) still exhibits more than double the maximum field amplitude of the resonance at λ = 610nm (Fig. 7(a)), since it originates from the branch corresponding to the localized dipole-image mode (Fig. 2(a)). In contrast with this plasmon hybridization, the odd SPP mode still shows a negligible spectral shift (staying centered at λ = 550nm) with varying particle length and negligible interaction with any localized modes (Fig. 8(b)), thus it does not play a role in the formation of any compound or hybridized plasmonic modes in such a system. This is simply due to the fact that the localized modes of this system are characterized by dipoles along the length of the particles and hence they can easily interact with the anti-parallel horizontally oriented field vectors of the even SPP mode in the Au film, but not the odd SPP mode.

#175682 - $15.00 USD Received 6 Sep 2012; revised 19 Nov 2012; accepted 29 Nov 2012; published 19 Dec 2012

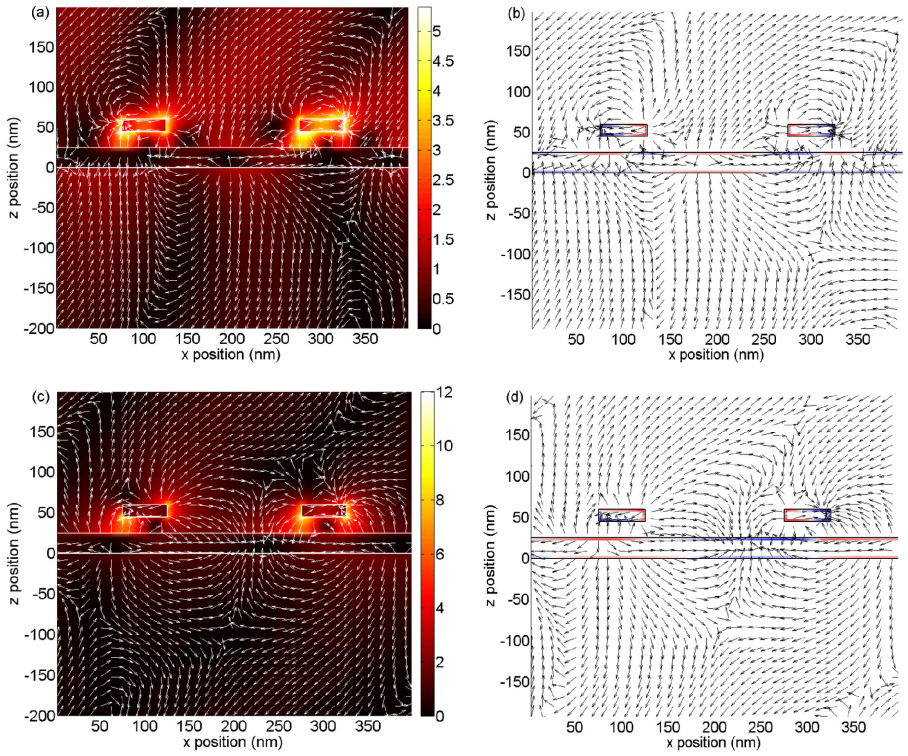

Fig. 7. Cross sections of the system shown in Fig. 1 with l = 50nm, showing (a) (Media 9), (c) (Media 11) time varying electric field amplitude and (b) (Media 10), (d) (Media 12) polarization charges via linked movies. Note the compound nature of both resonances for this particle size. (a,b) parallel hybridization combination of the even SPP and localized dipole-image mode for θ = 55° incidence, λ = 610nm. (c,d) anti-parallel hybridization combination of the even SPP and localized dipole-image mode for θ = 55° incidence, λ = 700nm.

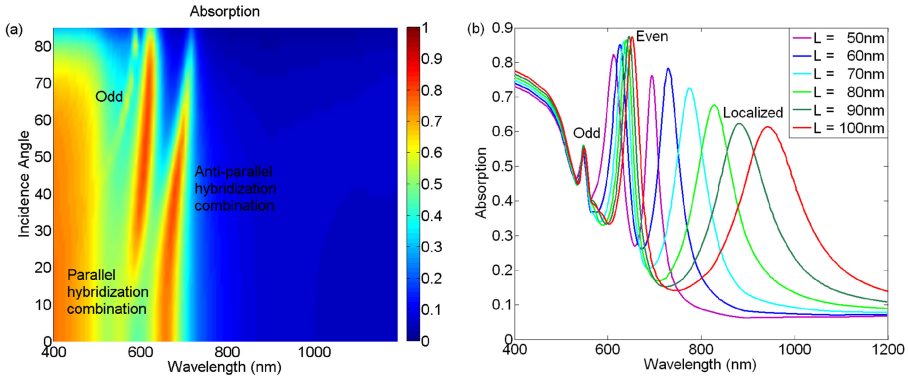

Fig. 8. (a) Absorption spectra of the system shown in Fig. 1 with a particle length of l = 50nm. Three absorption bands at λ = 550nm, 610nm, and 700nm for θ = 55° incidence correspond to the same odd SPP, even SPP, and localized dipole-image modes shown in Fig. 2 for a length of l = 100nm, however, now the last two bands have hybridized with a decrease in particle length, forming a parallel and anti-parallel combination of the two modes respectively. (b) Absorption spectra as a function of particle length from l = 50-100nm, while keeping the period constant to Λ = 200nm, for θ = 55° incidence. Note similar to Fig. 5, a shifting of the localized dipole-image mode and even-compound SPP with a decrease in particle length. The odd SPP mode, however, maintains the same spectral position.

#175682 - $15.00 USD Received 6 Sep 2012; revised 19 Nov 2012; accepted 29 Nov 2012; published 19 Dec 2012

5. Conclusion

In this communication, we have presented our computational findings on the compound plasmonic modes of a periodic Au grating array placed above a conducting Au film. A detailed study on the plasmon modes of this system was carried out as a function of both varying angle of incidence and wavelength. Excitation of a localized surface plasmon dipole-image mode was demonstrated, as well as excitation of two SPP modes via Bragg scattering. Furthermore, cross sections showing the time varying electric field profile and polarization charges illustrated the compound nature of the even SPP mode in the presence of a metallic grating, i.e. exhibiting both the characteristics of localized and propagating plasmon modes. These plots also illustrated additional hybridization of the even SPP mode with the localized dipolar plasmon mode of the system as the size of grating elements was reduced. The odd SPP mode, however, did not exhibit a compound nature or any plasmon hybridization and was shown to be solely due to Bragg scattering. Verification of the results was made through simulations with particle/grating element lengths varying from l = 50-150nm.

Acknowledgment

We are grateful to B. Gallinet for his support with the numerical simulations. Funding from the State Secretariat for Education and Research SER, and the Indian Department of Science and Technology (Grant no. INT/SWISS/P-16/2009) within the Indo-Swiss Joint Research Programme is gratefully acknowledged.

#175682 - $15.00 USD Received 6 Sep 2012; revised 19 Nov 2012; accepted 29 Nov 2012; published 19 Dec 2012